Heat and Mass Transfer
https://doi.org/10.1007/s00231-024-03464-1

ORIGINAL ARTICLE

Heat transfer on impingement cooled meshing spur gears: Experimental comparison of into-mesh, out-of-mesh and inclined impingement methods

Emre Ayan[1] · Christian Kromer[1] · Corina Schwitzke[1] · Hans-Jörg Bauer[1]

Received: 26 September 2023 / Accepted: 16 February 2024

Abstract
Oil jet impingement cooling is the standard approach to cool high-speed high-power gears. The heat transfer between oil jets and gears is experimentally investigated in this paper. The three established methods of oil jet impingement cooling -into-mesh, out-of-mesh and inclined impingement on one of the gears- are studied. Heat transfer coefficients for these methods are experimentally determined. A loss correction approach is implemented for the evaluation of measurements. For the inclined impingement method, heat transfer on the non-impinged gear and the influence of meshing on the heat transfer coefficient are investigated. Gear meshing has an insignificant effect on the average heat transfer coefficient over the gear tooth. However, the spatial distribution of the heat transfer coefficient depends on the meshing configuration. Significant cooling on the non-impinged gear is observed with the inclined impingement method. The inclined impingement method is superior to the into-mesh and out-of-mesh methods at all measured operating points.

Nomenclature

AF	Active flank
BL	Bottom land
c_p	Specific heat capacity
D_i	Impingement depth
d_n	Nozzle diameter
D_p	Penetration depth
E	Nozzle outlet eccentricity
h	Heat transfer coefficient
h^+	Relative local heat transfer coefficient
$\overline{h}$	Time and surface-averaged heat transfer coefficient
$\Delta\overline{h}_\%$	Deviation of average heat transfer coefficient from base configuration
L	Length of the path across one tooth
l_n	Nozzle length
m	Tooth module
N	Rotational speed
n_n	Number of nozzles
P	Driving power
$P_\mathrm{bearing,spin}$	Load-independent bearing losses
P_mv	Oil momentum variation losses
P_load	Load-dependent losses
P_loss	Total losses
P_spin	Load-independent losses
P_trapping	Trapping losses
P_windage	Windage losses
PF	Passive flank
$\dot{Q}$	Heat flow rate
$\dot{Q}_\mathrm{oil,trapping}$	Predicted oil trapping losses
$r_\mathrm{p,g}$	Geometrical pitch radius
$r_\mathrm{p,w}$	Working pitch radius
r_r	Root radius
r_spraybar	Spray bar axis offset
r_t	Tip radius
s	Circumferential coordinate
s^+	Dimensionless circumferential coordinate
S	Square error of calculated and measured temperatures
T_oil	Oil temperature
T_TC	Thermocouple temperature
$\mathbf{T}_\mathrm{cal}$	Calculated temperatures
$\mathbf{T}_\mathrm{mes}$	Measured temperatures
TL	Top land
u_jet	Oil jet velocity
$u_\mathrm{g,t}$	Circumferential speed of the gear at pitch radius
$\dot{V}_\mathrm{oil}$	Oil volume flow rate
W	Gear width

✉ Emre Ayan
emre.ayan@kit.edu

[1] Institute of Thermal Turbomachinery, Karlsruhe Institute of Technology, Karlsruhe, Germany

Published online: 29 February 2024

x	Profile shift
y	Axial coordinate
y^+	Dimensionless axial coordinate
Z	Tooth number

Greek symbols

α_n	Jet inclination
α_p	Pressure angle
ϵ	Angular distance between impingement and meshing
λ	Thermal conductivity
θ_m	Base positional angle
θ_v	Operational positional angle
ρ_{oil}	Oil density

1 Introduction

High-speed high-power gearboxes, similar to those found in modern geared turbofan aero-engines, are subject to substantial heat dissipation. The dissipated heat increases gear and lubricant temperatures, further deteriorating the lubrication quality and generating a positive feedback loop with ever-increasing temperatures within the gearbox. Therefore, a safe and reliable operation can only be assured with an adequate cooling system. Designing a cooling system capable of supplying sufficient cooling without giving rise to additional losses requires a comprehensive understanding of the heat transfer between the coolant and the gears.

Oil jet impingement cooling has been established as the primary approach for cooling in high-speed high-power gearboxes. However, the heat transfer between impinging oil jets and gears has not been studied extensively. The number of publications based on experimental thermal investigations is minimal. Townsend and Akin [1] aimed to experimentally capture the relation between the gear tooth temperatures and operating parameters. The oil jet was directed radially at one of the gears, and the impingement took place on the passive flank after the gear exited the meshing zone. The temperature on the active flank was measured after approximately 160° away from the meshing zone. An infrared microscope was utilized to measure the temperature. The experiments were carried out with varying rotational speeds and loads. They found that increasing the oil jet pressure leads to decreased gear surface temperatures, and increasing the rotational speed and load has shown the opposite outcome. Schober [2] focused on the oil jet impingement lubrication of gears. The aim was to study different impingement methods, into-mesh and out-of-mesh, and operating parameters to find the oil flow rate required for sufficient lubrication. Oil temperatures at the nozzle inlet and casing drain were measured. The bulk temperature of the pinion was measured after the test rig had come to a halt. The heat flow rate from gears into the oil was calculated via the nozzle and drain temperatures. It was only noted that this heat flow rate increases with increasing oil flow rate in an out-of-mesh configuration. Leoni [3] carried out temperature measurements with loaded gear pairs and varying lubrication and cooling configurations. The heat transfer coefficient was determined via finite element analysis (FEA) for a configuration. The constant total oil flow rate was divided into a lubricant flow, injected into-mesh, and a coolant flow, injected axially to the inner part of the gear. Increasing the lubricant flow increased the heat transfer coefficient on the gear tooth, and an increase in oil jet speed did not translate into a heat transfer coefficient increase if the heat transfer coefficient was defined with the oil injection temperature. The author noted that consideration of losses influences the accuracy of the results, and more accurate information about lubricant/coolant temperature in proximity of the gear and windage losses is essential for further refinement of thermodynamic calculation approaches. Handschuh [4] conducted an experimental study on oil jet lubrication of spiral bevel gears. The stationary temperatures were measured on a spiral bevel pinion instrumented with thermocouples. Transient data was collected via an infrared microscope. Oil flow rate and gear loading were varied in addition to the jet placement. Similar to previous outcomes, an increase in the load led to increasing temperatures on the pinion tooth, and an increase in the oil flow rate had the opposite effect. The lowest pinion temperatures were achieved when the oil jet was located to realize into-mesh or out-of-mesh impingement with no significant difference between them. Handschuh [5] has developed an FEA model to compare analytical results with the experiments. The heat transfer coefficient on the gear tooth was assumed since no data was available to the author. More recent publications on spiral bevel gears by Wang et al. [6], Zhang et al. [7], Gan et al. [8]; on spur gears by Wang et al. [9], Li and Tian [10] and Fernandes et al. [11]; on herringbone gears by Hu et al. [12] also had to utilize similar assumptions or greatly simplified models for the heat transfer coefficient on gear flanks, showing the lack of and need for experimental data in order to create accurate thermal models of transmission systems. An experimental method to investigate the heat transfer coefficient and its spatial distribution on a single spur gear was developed by von Plehwe et al. [13]. The influences of rotational speed and oil jet inclination on the heat transfer were discussed. The experimental method of von Plehwe et al. [13] was validated by Ayan et al. [14]. A second gear was included in the experimental setup by Ayan et al. [15] to investigate how meshing influences the heat transfer when inclined impingement is applied. The findings were limited by the influence of additional losses incurred by the meshing gears.

The aim of this study is to describe and quantify the cooling potential of oil jet impingement for applications

in high-speed high-power gearboxes. In order to investigate this cooling potential, the heat transfer between the oil and the gears should be isolated from other heat sources that arise due to meshing of two gears. The load dependent losses including the heat dissipation due to friction will be eliminated by conducting the experiments without load. The influence of the load independent losses cannot be easily eliminated since they exist as long as two meshing gears rotate and the oil is present. An empirical loss correction approach will be proposed in order to minimize the influence of these losses. The results of Ayan et al. [15] on inclined impingement will be reevaluated using the loss correction. Additionally, the secondary cooling effect on the non-impinged gear will be investigated. A comparison with the two other established impingement cooling methods, into-mesh and out-of-mesh, will also be carried out.

2 Experimental setup

The experimental setup [13, 14, 17] shown in Fig. 1 can be divided into three main groups of components: oil supply, cooling air supply and rotational components. The oil supply consists of two oil cycles. The first cycle keeps the oil in the oil reservoir at the desired temperature using a gear pump and a temperature regulated heater. The second cycle is used to feed the oil from the oil reservoir into the spray bar. The feed pump is controlled using the flow meter downstream to deliver the required oil flow rate. The oil is fed back from the casing into the reservoir using a return pump. The cooling air is supplied via a side-channel blower into the plenum chamber. The cooling air temperature is decreased below the ambient temperature using a heat exchanger upstream of the chamber. Twenty hoses connect the plenum chamber to the cooling cylinder, from which the air jets are ejected onto the inner surface of the instrumented gear. The instrumented gear is mounted on a shaft connected to an electrical motor together with a sensor unit to measure the torque and rotational speed of the shaft. A telemetry sender is attached to the instrumented gear. The ends of thermocouples are soldered onto the circuit board of the telemetry sender. The voltage data required for temperature measurements are transferred digitally from the rotating sender into the stationary receiver unit during operation. A PT100 thermistor located on the circuit board of the sender is utilized to determine the cold junction temperature.

The experimental setup includes a second gear driven by the instrumented gear for measurements with meshing configurations. The non-instrumented driven gear (green in Fig. 2) is made of C45 steel. The instrumented driving gear (black in Fig. 2) is made of TiAl6V4 and is instrumented with thermocouples on its outer and inner surfaces. In contrast to a real world cooling application, the heat transfer is inverted in the experimental setup with the oil utilized as the heat source. The outer surface of the instrumented gear is heated by the impinging oil jets (orange in Fig. 2) and the inner surface is cooled via air jet impingement (blue in Fig. 2). The inversion of heat transfer means that the oil temperature and therefore the oil viscosity will decrease after the impingement in contrast to the cooling application where the opposite effect will be observed. This might have an impact on the transferability of the results due to differences in tooth surface wetting. However, the inversion is in the first place necessary to even realize an oil temperature and an oil viscosity, which closely represent the real world application. Using the oil with $T_{oil} = 80$ °C as the heat sink would require a substantially higher inner surface temperature. However, the telemetry sender is rated for a maximum temperature of 80 °C and started to display inconsistent behavior above 60 °C in operation. The alternative would be to keep the oil temperature very low, which would drastically reduce the transferability of the results due to the exponential increase of viscosity for decreasing temperatures [16].

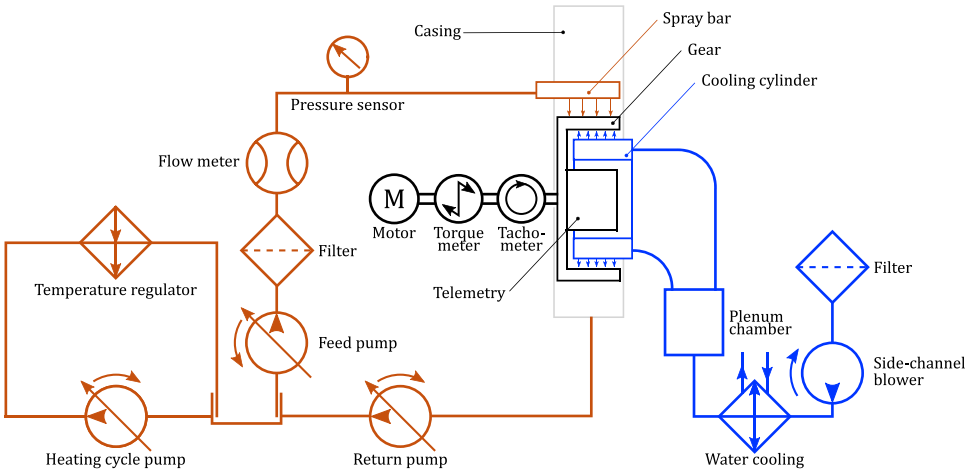

Fig. 1 Layout of the experimental setup, where the components associated with the oil and cooling air supply are depicted in orange and blue, respectively. The components in black belong to the rotatory components in the setup. The non-instrumented gear is not depicted. The casing of the test rig is shown in gray

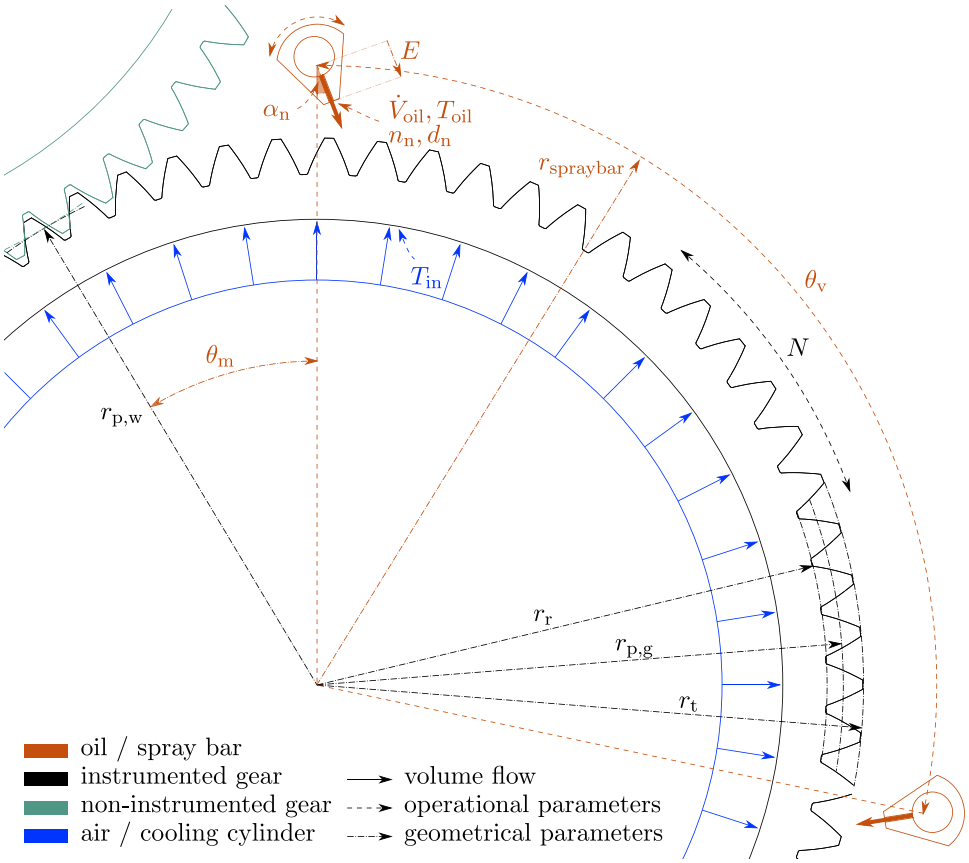

Fig. 2 The experimental setup with the spray bar in orange, the instrumented driving gear in black, the non-instrumented driven gear in green, and the cooling cylinder in blue. The oil and air jets are depicted with the solid arrows, the variable operational parameters with the dashed lines and dashed arrows, and the constant geometrical parameters with the dot-dashed arrows [15]

The outer surface of the instrumented gear is schematically pictured in Fig. 3 with four cylindrical oil jets. Eighteen outer thermocouples and three inner thermocouples on one-eight of the gear are utilized for the measurements, depicted in red for the outer surface and blue for the inner surface in Fig. 3. The outer surface is transformed into the tooth coordinate system with the normalized axial and circumferential coordinates y^+ and s^+. The spatial heat transfer coefficient distribution will be presented in this coordinate system. Each outer thermocouple is placed on a different tooth to realize the instrumentation required for the desired spatial resolution. This is possible since the oil jet impingement and the stationary heat transfer should be identical for each tooth. Furthermore, the thermocouples are placed only on one-eight of the gear since the wetting and the stationary heat transfer should be symmetrical on both halves of a tooth quarter with the impingement occurring in the middle of the tooth quarter.

A groove is cut into the respective tooth to place a type K thermocouple with a sheath diameter of 0.25 mm at its position. The thermocouple is laid into the groove and covered

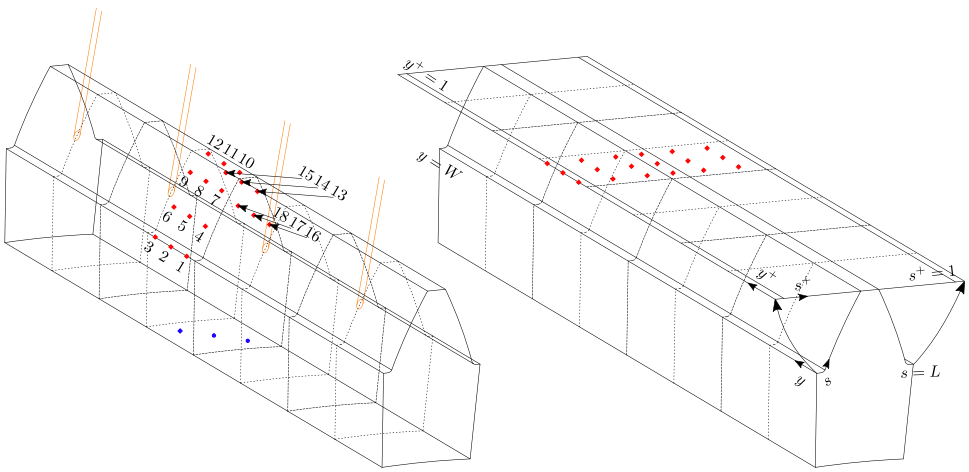

Fig. 3 One gear tooth with the cylindrical oil jets in orange, the outer thermocouples in red and the inner thermocouples in blue. The tooth coordinate system is shown on the right side [14]

Fig. 4 An outer thermocouple embedded into the groove and covered with the adhesive [17]

with an high temperature adhesive, that has a thermal conductivity of $\lambda_{\text{adhesive}} = 5.7\ \text{W/(mK)}$, which is only slightly lower than the conductivity of the gear material $\lambda_{\text{TiAl6V4}} = 7\ \text{W/(mK)}$. The adhesive is manually sanded after it is cured to match the height of the groove and minimize the deviations from the original tooth surface. The final appearance of an outer thermocouple is depicted in Fig. 4.

The iterative evaluation approach, initially developed by von Plehwe et al. [13] and improved by Ayan et al. [14], is employed to determine the heat transfer coefficient using measured temperatures (Fig. 5a). The FEA model utilized for the evaluation is depicted in Fig. 5b. It consists of 179489 tetrahedral elements with a maximum element size of 1 mm. The circumferential boundaries between the modelled tooth and its neighbouring teeth are modelled as periodic boundaries. Only one tooth quarter is modelled making use of the aforementioned symmetry assumptions. The mean temperature of the inner thermocouples is applied as a uniform boundary condition on the inner surface. An initial heat transfer coefficient distribution is applied on the tooth surface in the first iteration of the evaluation. Temperatures from the FEA calculation ($\mathbf{T}_{\text{cal}}$) are compared against the measured temperatures ($\mathbf{T}_{\text{mes}}$). The estimated spatial heat transfer coefficient distribution is iteratively improved via the Levenberg-Marquardt method [14] until the differences between the calculated and measured temperatures are minimized so that the convergence condition

$$S = (\mathbf{T}_{\text{mes}} - \mathbf{T}_{\text{cal}})^{\text{T}}(\mathbf{T}_{\text{mes}} - \mathbf{T}_{\text{cal}}) < 18 \cdot 10^{-4}\ \text{K}^2 \tag{1}$$

is fulfilled. The FEA calculations are carried out using the PARDISO solver and the COMSOL Multiphysics® software.

Temperature measurements are taken and averaged over 30 s after waiting for at least 7 min for the operating point to reach the stationary state, where a temperature's rolling average over 30 s does not vary more than 0.1 K within a minute. A preliminary study with single gear measurements have shown that the surface-averaged heat transfer coefficients are within ±2.5% of the stationary state after a waiting period of 3 min (Fig. 6). In the preliminary study, the last

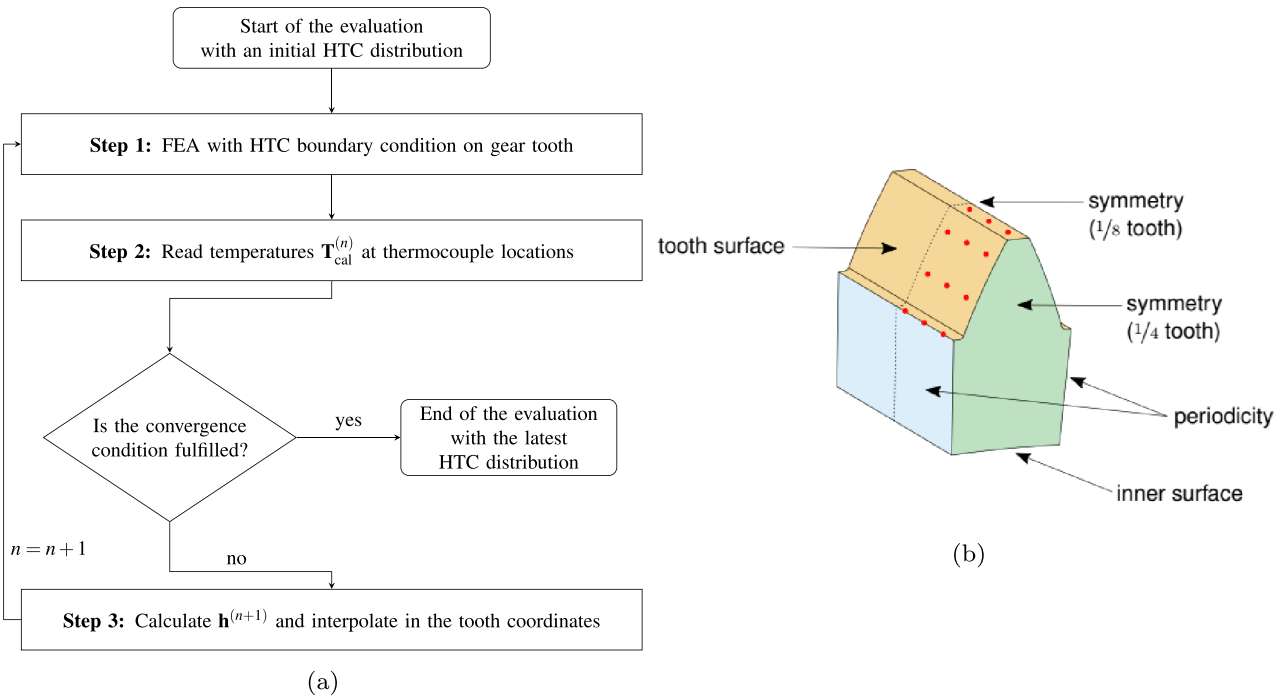

Fig. 5 Employed iterative evaluation algorithm as a flow diagram (**a**) and the FEA model (**b**) [14]

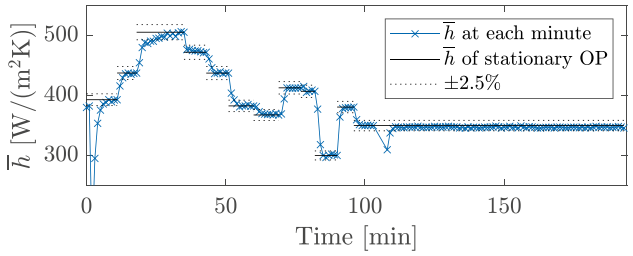

Fig. 6 Preliminary study to assess the time required for stationary measurements. The solid lines mark the heat transfer coefficients determined with the measurements at the stationary point according to the experimenter. The dashed lines form an interval of ±2.5% around the stationary heat transfer coefficient. Each marker shows a heat transfer coefficient that is determined with the temperatures measured in the last 30 s

operating point is measured for 97 min, with a 4 min break between 104th and 108th minutes. The test rig is switched off in this interval. The heat transfer coefficient increases up to the stationary value within 3 min of restarting the experiment.

An assessment of the measurement uncertainty is extremely challenging due to the complex dependency of the heat transfer coefficient on individual temperature measurements. von Plehwe et al. [13] conducted a Monte Carlo study based on single gear experiments, which resulted in a standard deviation of 3.76% for the surface-averaged heat transfer coefficient. However, the inclusion of meshing into the experiments further complicates the uncertainty assessment as discussed in the following sections.

A total of ten configurations are selected for investigation. These configurations are shown in Fig. 7. The letter C and the following number represent the individual configurations. The last letter indicates the rotational direction of the instrumented gear, with L representing the counterclockwise and R representing the clockwise rotation of the instrumented gear. C0 is the inclined impingement cooling configuration without gear meshing. C1 is the inclined impingement cooling configuration with gear meshing and the operational positional angle $\theta_v = 0°$. C2 is the inclined impingement cooling configuration with gear meshing and $\theta_v = 102°$. C3 is the inclined impingement cooling configuration with gear meshing and oil jet impingement on the non-instrumented gear. C4R and C4L are the out-of-mesh and into-mesh configurations, respectively. For each configuration, measurements are carried out at four flow rates (3.2; 3.66; 4; 4.4 L/min) and three rotational speeds (2000; 3000; 4000 RPM). These rotational speeds result in circumferential speeds of 27.23, 40.84 and 54.45 m/s at the geometrical pitch radius. The jet inclination α_n is kept constant at 20° in the rotational direction of the impinged gear at the impingement location for configurations C0, C1, C2 and C3. For C4, the jet is directed tangentially onto the pitch circle. Measurements with C1 and C2 configurations are utilized to investigate the influence of meshing on the inclined impingement (Section 4.1). Results with C3 configurations are compared against those with C1 configurations to assess the heat transfer on the non-impinged gear (Section 4.2). Comparison of impingement methods is carried out using measurements with C4, C1L and C3L configurations (Section 4.3).

The geometrical and operational parameters of the experimental setup are summarized in Table 1.

3 Empirical loss correction

Ayan et al. [15] have shown that a direct determination of the heat transfer coefficient with the established evaluation approach has only limited validity for meshing configurations with unloaded gears. The evaluation resulted in extremely high heat transfer coefficients, which cannot be explained by the influence of meshing on the heat transfer alone. For the C1R configuration, only a minimal difference

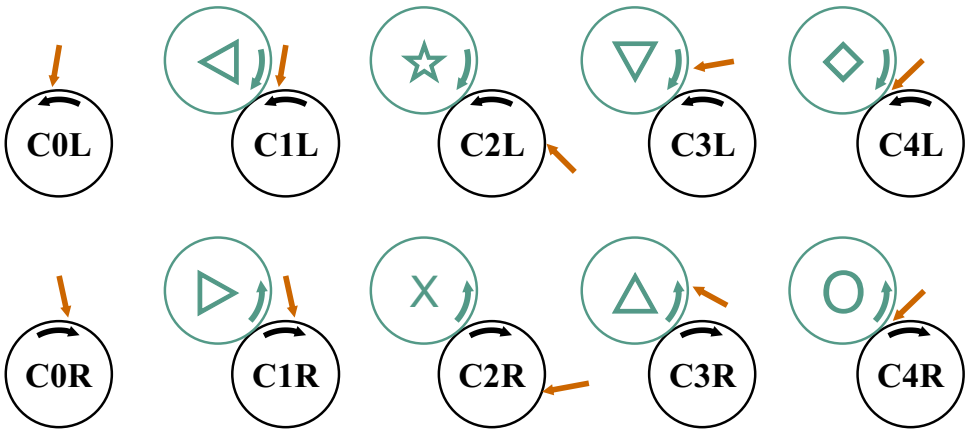

Fig. 7 Investigated configurations with the instrumented gear in black, the non-instrumented gear in green and the oil jet in orange. The rotational directions are shown with the arrows within the circles. The green markers are used for the respective configuration in the results section

Table 1 Geometrical and operational parameters of the experimental setup

Parameter	Symbol	Value
Number of teeth	Z	65
Tooth module	m	4 mm
Pressure angle	α_p	25°
Profile shift	x	+1 mm
Gear width	W	90 mm
Root radius	r_r	126 mm
Tip radius	r_t	135 mm
Geometrical pitch radius	$r_{p,g}$	130 mm
Working pitch radius	$r_{p,w}$	131.35 mm
Spray bar axis offset	$r_{spraybar}$	153 mm
Base positional angle[a]	θ_m	30.85°
Operational positional angle	θ_v	0° or 102°
Number of nozzles	n_n	4
Nozzle diameter	d_n	0.82 mm
Nozzle length	l_n	4.8 mm
Nozzle outlet eccentricity	E	9.8 mm
Jet inclination for inclined impingement[b]	α_n	20°
Oil temperature	T_{oil}	80 °C
Oil volume flow rate	$\dot{V}_{oil}$	3.2; 3.66; 4 or 4.4 L/min
Rotational speed	N	2000; 3000 or 4000 RPM
Circumferential speed at $r_{p,g}$	$u_{g,t}$	27.23; 40.84 or 54.45 m/s

[a]At this position, the distance between the centre of the non-instrumented gear and the spray bar is also $r_{spraybar}$

[b]The positive jet inclination is defined in the same direction as the tangential velocity of the impinged gear at the impingement point

from the heat transfer coefficient of C0R is expected since the impinged gear completes 91.4% of its rotation before entering the meshing zone. The influence of gear meshing on the heat transfer should be weakest here since the spreading of the oil film and the decrease of the oil volume due to fling-off, and thus also the heat transfer between the oil and the gear, have progressed further than in other configurations, even if not entirely completed. Nevertheless, at 4000 RPM, an increase of up to three times in the time and surface heat transfer coefficient is observed between C1R and C0R.

A possible reason for this high discrepancy is the occurrence of new losses due to meshing. These were investigated via additional measurements. It was found that the trapping losses $P_{trapping}$, which consist of air pocketing/pumping and oil squeezing, correlate strongly with the heat transfer coefficient discrepancy. The trapping losses in the experiments were determined by subtracting the windage losses $P_{windage}$, the load-independent bearing losses $P_{bearing,spin}$ and the momentum variation losses due to oil deflection P_{mv} from the driving power

$$P = P_{loss} = \underbrace{P_{load}}_{=0} + P_{spin} = P_{windage} + P_{bearing,spin} + P_{mv} + P_{trapping}, \tag{2}$$

with total losses P_{loss}, load-dependent losses P_{load} and load-independent losses P_{spin} [15].

Correcting the influence of trapping losses is a major challenge because critical questions like what part of these losses can be attributed to which medium, whether the heat dissipated within the oil film remains there or gets transferred away by the gears, and how much oil is present on the gear during meshing are challenging to answer. An empirical loss correction approach is implemented in this study to enable a realistic comparison of different configurations, even if the correction does not result in quantitatively very accurate results.

For the operating points with $N = 4000$ RPM, the evaluation algorithm converges to solutions where the total heat flow rate into the instrumented gear over the outer surface and out of the instrumented gear over the inner surface[1] is, in fact, greater with C0R (Table 2) than with C1R. This indicates that the extra heat dissipated by the trapping losses does not leave the test rig directly by means of air jet impingement cooling. The heat transfer over the non-instrumented gear can also be neglected since it is not actively cooled. In a time-averaged steady-state consideration, the heat dissipated within the oil film could be regarded as if it remains within the oil volume. Therefore, the influence of the trapping losses can be modelled by increasing the effective oil temperature in the evaluation algorithm. The experimentally determined trapping losses cannot be used directly to model this change since they also include the losses generated by air trapping. The assumption of equal heat transfer coefficients for C0R and C1R is utilized to derive the empirical loss correction. Based on this assumption, iterative finite element calculations are performed. The evaluation algorithm of Ayan et al. [14] is modified to use the heat transfer coefficient distributions of C0R cases and find effective oil temperatures $T_{oil,eff}$ for the corresponding C1R cases so that the discrepancies between the measured and simulated gear temperatures with C1R are minimized.

Table 2 Calculated losses and heat flow rates for C0R and C1R at $N = 4000$ RPM

$\dot{V}_{oil}$	$P_{trapping}$	$\dot{Q}_{in,out,C0R}$	$\dot{Q}_{in,out,C1R}$
3.2 L/min	767.22 W	496.89 W	489.66 W
3.66 L/min	760.83 W	535.74 W	512.53 W
4 L/min	771.40 W	544.16 W	521.37 W
4.4 L/min	776.74 W	555.00 W	524.06 W

[1] These heat flow rates are equal for the stationary solution.

The oil trapping losses that would be required for the determined temperature increase are then calculated using

$$\dot{Q}_{\text{oil,trapping}} = (T_{\text{oil,eff}} - T_{\text{oil,C1R}})\dot{V}_{\text{oil}}\rho_{\text{oil}}c_{\text{p}} \tag{3}$$

with oil density ρ_{oil} and specific heat capacity c_{p} at the measured oil temperature $T_{\text{oil,C1R}}$, assuming the whole oil volume experiences the temperature increase.

The experimentally determined total trapping losses of C1R measurements and with Eq. 3 predicted oil trapping losses are depicted in Fig. 8 together with their fitted functions, which is

$$\dot{Q}_{\text{oil,trapping,fit}} = 1.246 \cdot 10^{-8} \cdot \frac{N}{\text{RPM}}^{2.962} \text{W} \tag{4}$$

for the predicted oil trapping losses. The non-existence of a dependency of $\dot{Q}_{\text{oil,trapping}}$ on the oil volume flow rate is visible in Fig. 8, especially at $N = 4000$ RPM. Additionally, the fitting functions for the total trapping losses of different configurations are plotted in Fig. 9. The trapping losses of configurations C1L, C2L and C3L are notably different than C1R, even though the configurations are quite similar in their setup. On the contrary, two of the most different configurations, C1L and C3R, have fitting functions that are very close to C1R. Partitioning the determined losses into oil and air losses is unrealizable and no clear correlation between the total trapping losses and the configurations is found. The best possible approach is to use Eq. 4 to calculate an effective oil temperature for each measurement with a meshing configuration. The effective oil temperature is then used in the evaluation instead of the measured oil temperature. For configurations with impingement shortly before meshing (C1L, C2L, C3L, C4L), the oil volume with the dissipated heat will have a higher temperature during

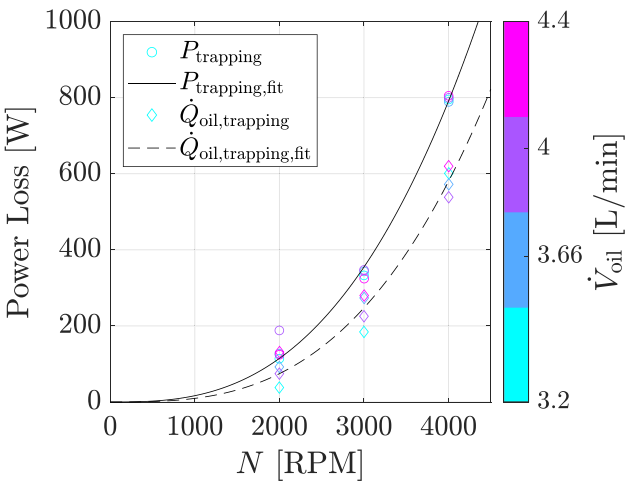

Fig. 8 Determined total trapping losses P_{trapping} and predicted oil trapping losses $\dot{Q}_{\text{oil,trapping}}$ for C1R cases

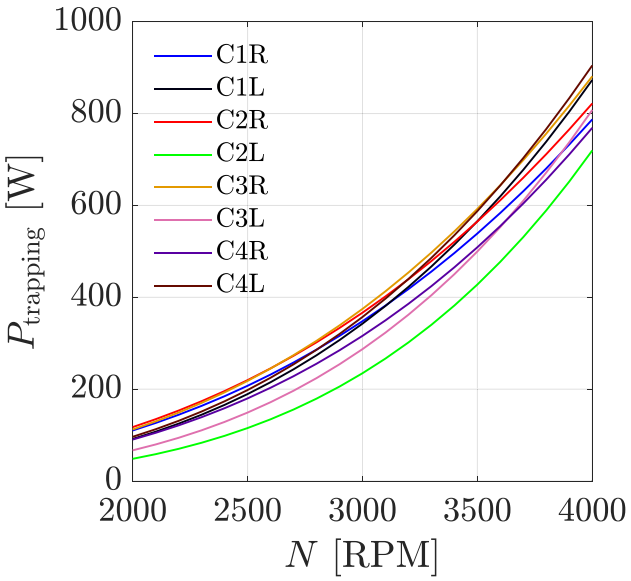

Fig. 9 Fitted functions for the determined total trapping losses P_{trapping} of meshing configurations

nearly the whole rotation until the next oil jet impinges. For configurations with impingement shortly after meshing (C1R, C2R, C3R, C4R), the oil film will initially have a much-increased temperature since the remaining oil volume during meshing will be lower compared to the L configurations after the rotation. It is assumed that the excessive heat stays within the oil film until the new oil jet impinges on the gear and the new oil volume mixes with the settled oil film, transferring the dissipated heat over to the total oil volume as in the case with L configurations. The assumption that the total oil volume experiences the dissipated heat is most likely not true since it was shown numerically by Keller et al. [18] that nearly half of the oil volume gets splashed away from the tooth immediately after the impingement at their simulated operating point. This splashed away oil volume would not experience the dissipation during meshing in L configurations. Also, there would not be any time for it to take part in the heat transfer with the settled oil film in the R configurations since it splashes away immediately after the impingement. Accounting for this splashed away oil volume would change the predicted oil trapping losses calculated with Eq. 3. However, if the splashed away oil volume ratio is also assumed to be the same for all operating points, this would not affect the determined effective oil temperatures since the fitting function in Eq. 4 would also change accordingly. A more accurate, case-specific assessment depending on the splashed away oil volume is impossible with the current state of knowledge.

Another weakness of the utilized loss correction model is observed in measurements with the C3 configurations. At the highest rotational speed, $N = 4000$ RPM, the heat

transfer coefficient on the non-impinged gear seems to be higher than on the impinged gear (see Section 4.2). In configurations C1, C2 and C4, the heat transfer between the oil and the instrumented gear can be evaluated uncoupled from the non-instrumented gear, assuming that no heat transfer occurs between the non-instrumented gear and the oil film or the instrumented gear. The non-instrumented gear would obviously be in direct contact with the oil film during meshing, but this contact time is considered too short for a considerable heat transfer to take place. In configuration C3, however, the oil jet first impinges on the non-instrumented gear. The non-instrumented gear is not cooled actively and may have a nearly uniform tooth temperature very close to the oil film temperature after meshing, including the temperature increase due to oil trapping. The new impinging oil volume would therefore be firstly heated up by the uncooled gear before even getting into the meshing zone and in contact with the instrumented gear. This means that additional consideration of the heat flowing from the non-instrumented gear into the oil volume and indirectly influencing the effective oil temperature experienced by the instrumented gear is required. Therefore, the discussion of C3 results will only focus on the measurements with the lowest rotational speed, where the trapping losses and the influence of model weaknesses are minor.

4 Results

The results will be investigated in three groups in the following. The first group consists of configurations C1 and C2 to assess how meshing influences heat transfer with the inclined impingement method. The second group is for the comparison of C1 and C3 configurations, where the latter represents the heat transfer on the secondary, non-impinged gear by having oil jets impinging on the non-instrumented gear. The third group is formed by configurations C4R, C4L, C1L and a combination of C1L and C3L to evaluate the heat transfer potentials of the three established impingement cooling methods of out-of-mesh, into-mesh and inclined impingement. For each configuration, the time and surface averaged heat transfer coefficient will be discussed with a normalized difference to the non-meshing configuration C0j with the same rotational direction:

$$\Delta\overline{h}_{\%,\mathrm{Cij}} = \frac{\overline{h}_{\mathrm{Cij}}}{\overline{h}_{\mathrm{C0j}}} - 1,\ i \in \{1,2,3,4\},\ j \in \{\mathrm{L},\mathrm{R}\}. \tag{5}$$

The spatial distribution of the heat transfer coefficient can be explored with the help of heat transfer maps. These maps display the heat transfer coefficient over the tooth surface in the tooth coordinate system. The local heat transfer coefficient is normalized with the average heat transfer coefficient of the corresponding operating point without meshing:

$$h^{+} = \frac{h_{\mathrm{Cij}}}{\overline{h}_{\mathrm{C0j}}},\ i \in \{1,2,3,4\},\ j \in \{\mathrm{L},\mathrm{R}\}. \tag{6}$$

Figures 10 and 11 show the heat transfer maps for all investigated configurations at operating point 1 (OP1, $\dot{V}_{\mathrm{oil}} = 3.2\,\mathrm{L/min}$, $N = 2000\,\mathrm{RPM}$) and operating point 2 (OP2, $\dot{V}_{\mathrm{oil}} = 3.2\,\mathrm{L/min}$, $N = 4000\,\mathrm{RPM}$), respectively. The y-axis, y^{+}, is limited between $0.5 \leq y^{+} \leq 0.75$, showing only one tooth quarter, with the oil jet impinging along the line $y^{+} = 0.625$. The vertical white lines on the map are the transition lines between different parts of the tooth geometry, which are the bottom land (BL), the active flank (AF), the top land (TL), and the passive flank (PF). $s^{+} = 0$ corresponds to the centre of one bottom land and increases to $s^{+} = 1$, where the centre of the following bottom land is reached. In order to keep the active flank always on the left side of the image for more straightforward comparability, the x-axes of the heat transfer maps of clockwise rotating configurations (CiR) are inverted.

4.1 Influence of meshing on the inclined impingement

The first group consists of the configurations C1L, C1R, C2L, and C2R. It allows an investigation of the influence meshing has on the heat transfer utilizing the variable angular distance ϵ between impingement and meshing locations. This distance is defined as the ratio of the angular dimension between the nozzle position and the pitch point to the entire pitch circle with

$$\epsilon = \frac{|k - \theta_{\mathrm{m}} + \theta_{\mathrm{v}}|}{360°},\ k = \begin{cases} 360°, & \text{if CiR.} \\ 0°, & \text{if CiL.} \end{cases} \tag{7}$$

The resulting values for ϵ are $\epsilon_{\mathrm{C1L}} = 8.6\%$, $\epsilon_{\mathrm{C1R}} = 91.4\%$, $\epsilon_{\mathrm{C2L}} = 36.9\%$ and $\epsilon_{\mathrm{C2R}} = 63.1\%$. The a priori expectation is that an increased influence of meshing should be observed with a decrease in ϵ. There will be less time available for the heat transfer between the oil and the gear to occur before the engaging teeth transforms the oil film if the distance between impingement and meshing is decreased. The engaging teeth should squeeze the oil film out, which is initially centred around the impingement location and create a more uniform wetting on the active flank of the tooth. This squeezing out of the oil film may improve the heat transfer by generating a larger wetted area but may also decrease the heat transfer if some of the oil is transferred over to the non-impinged gear or squeezed out of the tooth gap completely, decreasing the oil volume available to the instrumented gear. This expected

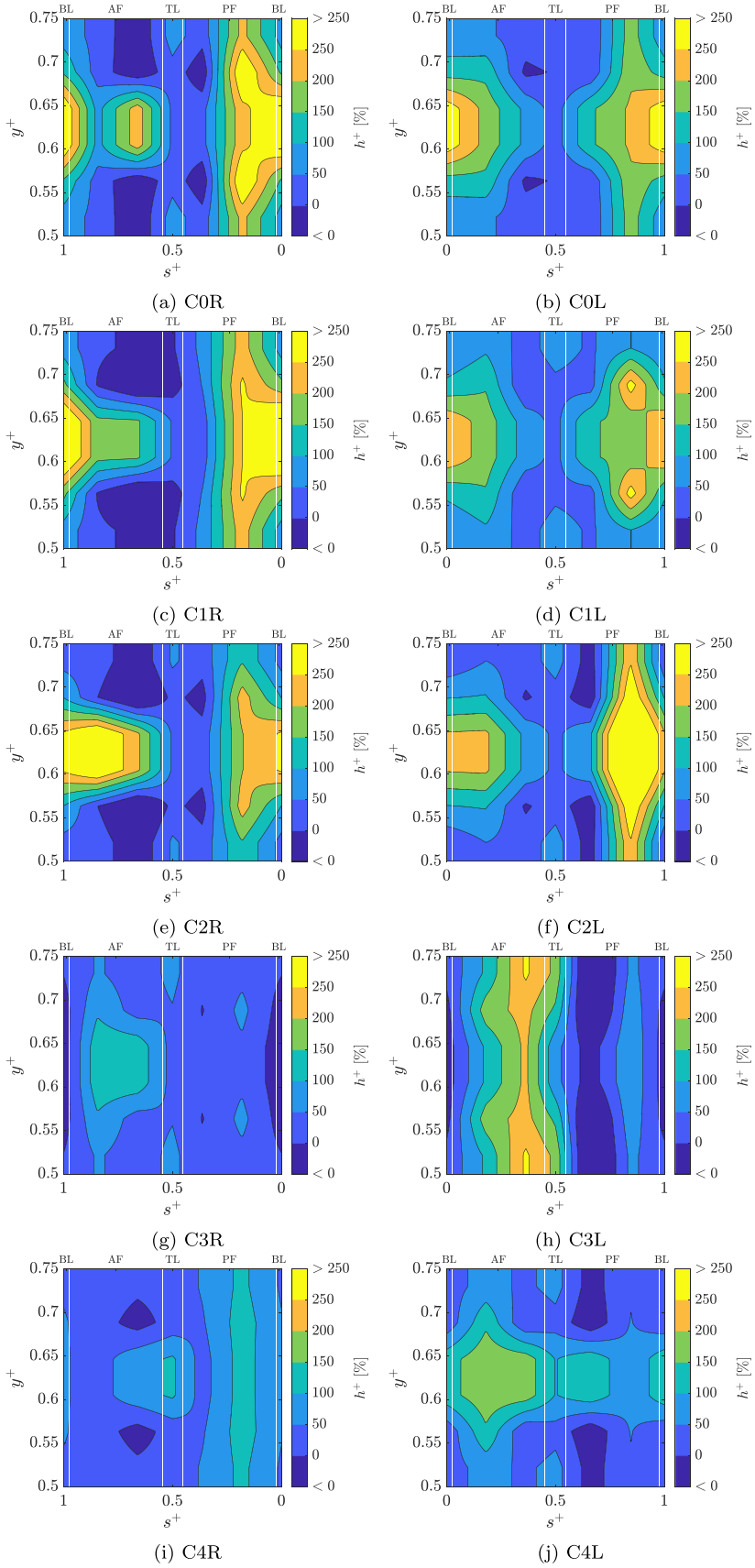

Fig. 10 Heat transfer maps at OP1 with $\dot{V}_{\text{oil}} = 3.2$ L/min, $N = 2000$ RPM

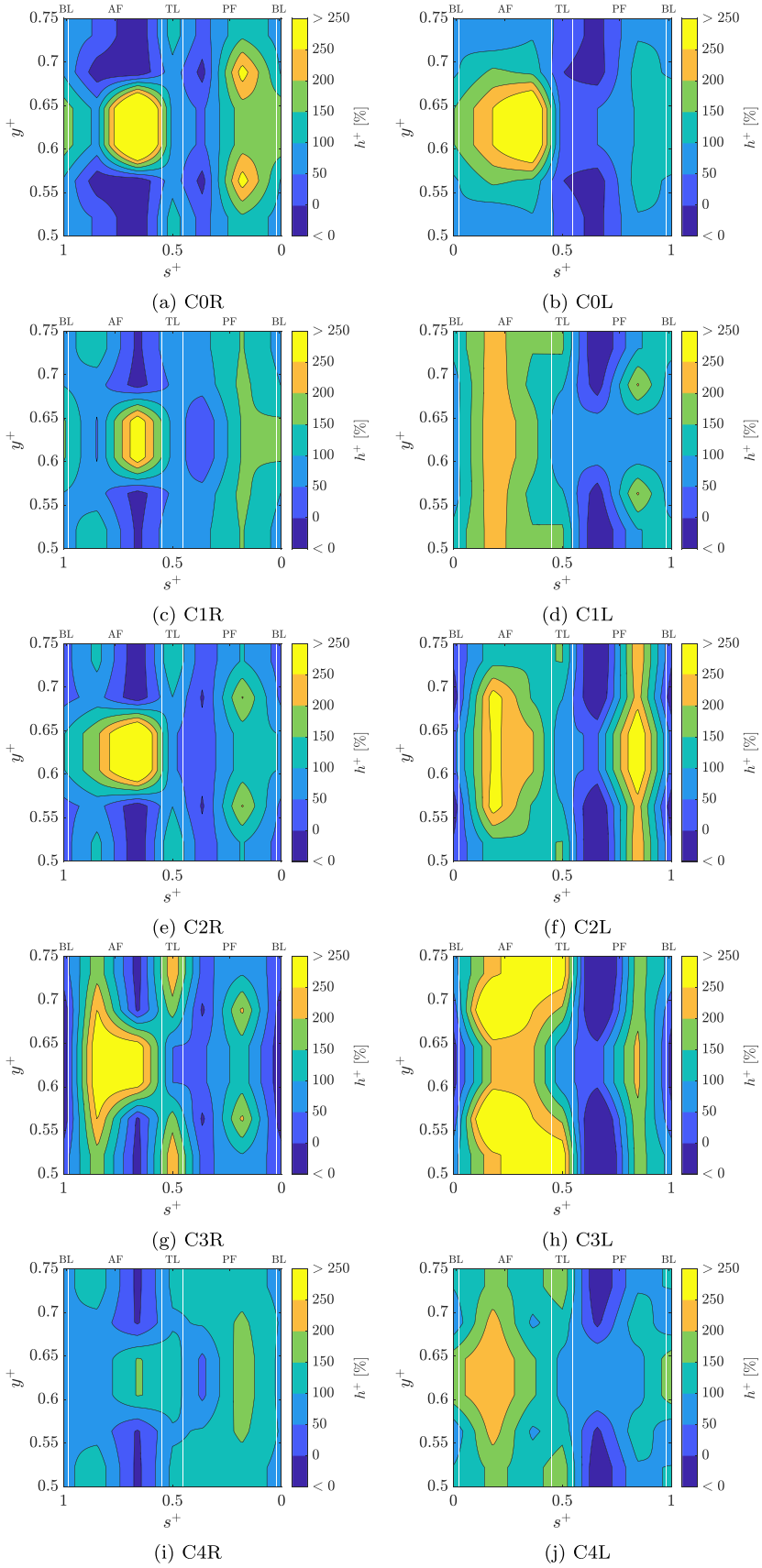

(a) C0R (b) C0L

(c) C1R (d) C1L

(e) C2R (f) C2L

(g) C3R (h) C3L

(i) C4R (j) C4L

Fig. 11 Heat transfer maps at OP2 with $\dot{V}_{\text{oil}} = 3.2$ L/min, $N = 4000$ RPM

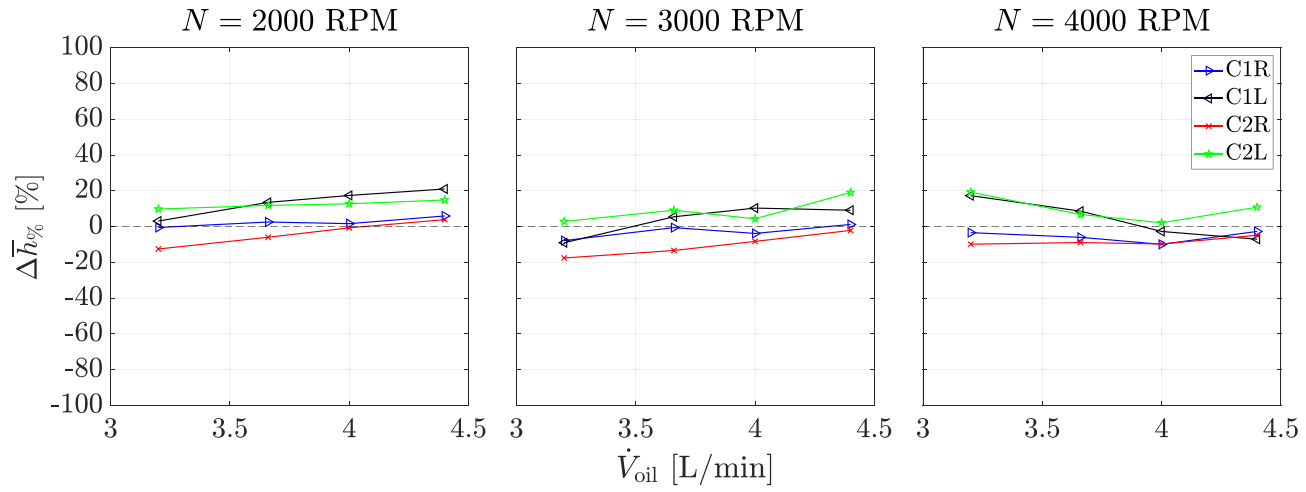

Fig. 12 $\Delta\bar{h}_{\%}$ for configurations C1R, C1L, C2R and C2L

influence of meshing will be discussed regarding the surface averaged heat transfer coefficient and its spatial distribution.

Figure 12 shows $\Delta\bar{h}_{\%}$ of the investigated configurations with a variation of rotational speed N and oil volume flow rate $\dot{V}_{\mathrm{oil}}$. No clear dependence on the configuration is found for the surface averaged heat transfer coefficient. With the decreased accuracy of the meshing measurements, where the effective oil temperature is corrected using a presumptive approach, a null hypothesis stating that the gear meshing does not influence the average heat transfer coefficient cannot be rejected. The expected change in influence with ϵ is not observed for any of the rotational speeds and volume flow rates. In this regard, the results are summarized as a box plot in Fig. 13. Here, each box and its antennas contain the $\Delta\bar{h}_{\%}$ values for the respective configuration. The medians of both extremes, C1L and C1R, are 8.9% and −1.6%, respectively, and thus differ only slightly. Moreover, contrary to the expectation, the medians of the C2 configurations are not between those of C1L and C1R, with 10.3% and −8.6% for C2L and C2R, respectively.

The non-meshing measurements with C0R (Figs. 10a and 11a) and C0L (Figs. 10b and 11b) result in slightly different heat transfer maps, which can be explained by the different sets of thermocouples located on the active flank where the oil jet impinges on.[2] The qualitative distribution of heat transfer coefficient for a given operating point is, however, similar. For each operating point, the heat transfer on the active flank is concentrated axially in the centre ($y^+ = 0.625$) resembling the path followed by the oil jet. For OP1, this region stretches from the first bottom land up to the top land. The impingement depth, calculated with the model of Akin et al. [19], is $D_{\mathrm{i}} = 4.2$ mm, meaning that the impingement starts at $s^+ = 0.25$ for C0L and $s^+ = 0.75$ for C0R. As shown by Keller et al. [18], the oil can penetrate further into the tooth gap after the impingement, with penetration depths reaching $D_{\mathrm{p}} \approx 2D_{\mathrm{i}}$. This explains how the bottom land of the tooth experiences the observed high heat transfer. There is also high heat transfer observed on the passive flank, suggesting a good oil wetting here, which shows

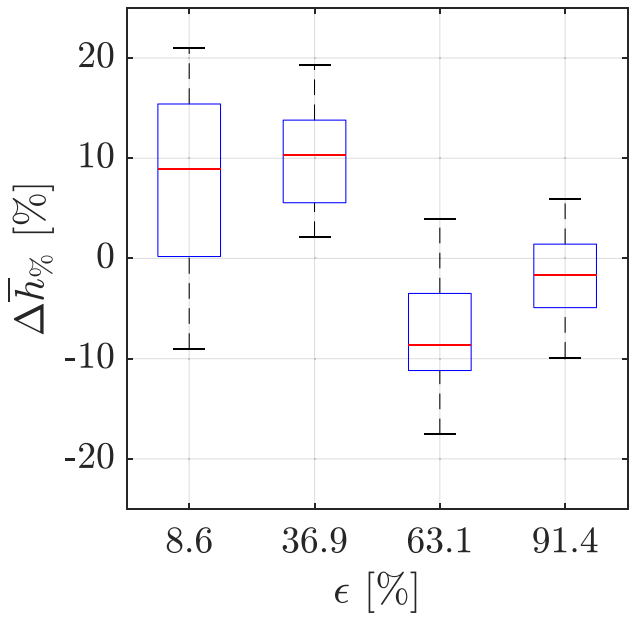

Fig. 13 $\Delta\bar{h}_{\%}$ with varying ϵ

[2] It should be noted that the average heat transfer coefficients of these measurements only differ by 0.9% and 3.1% at OP1 and OP2, respectively.

that some of the impinging oil either splashes from the active flank onto the passive flank after the impingement or curves up at the bottom land and propagates further on the passive flank. For OP2, the high heat transfer region on the active flank is more localized near the top land, which can be explained by the low impingement depth of $D_i = 2.2$ mm, meaning that the impingement starts at $s^+ = 0.35$ for C0L and $s^+ = 0.65$ for C0R. The oil film seems to penetrate less than at OP1 since the increased rotational speed exhibits a stronger counterforce. A considerable amount of heat transfer is still present at the passive flank, which can possibly be attributed to oil splashing after the impingement since the high heat transfer region is not continuous, as is the case at OP1.

The axial concentration on the active flank is also apparent in C1R (Figs. 10c and 11c) and C2R (Figs. 10e and 11e) configurations with relatively large ϵ values. This can be attributed to the fact that even for C2R, the heat transfer process is mostly complete by the time of engagement. A possible change in the oil wetting by the teeth does not cause any observable effect on the temperature field and the heat transfer coefficient distribution on the active flank. From heat transfer maps of C1L (Figs. 10d and 11d) and C2L (Figs. 10f and 11f), it can be deduced that the uniformity of heat transfer coefficient distribution in the axial direction increases with decreasing ϵ and increasing N. If the counterclockwise rotating configurations are compared, the gradients on the active flank are steeper with C0L compared to the more gradual decrease with C1L. The difference is much more apparent at OP2, where the axial width of the high heat transfer region increases considerably with decreasing ϵ. The increased uniformity in axial distribution is likely because the heat transfer is not completed or saturated enough before the oil film is affected by the teeth. The time available for the heat transfer will also be halved by doubling the rotational speed, which explains the difference between OP1 and OP2. It should be noted that the increased uniformity on the active flank does not explain the relatively significant difference between the average heat transfer coefficients of counterclockwise and clockwise rotating configurations at OP2, shown in Fig. 12. Other operating points with $N = 4000$ RPM exhibit the change in axial uniformity consistently even though there is less difference in the average heat transfer coefficients.

4.2 Secondary heat transfer on the non-impinged gear

The secondary cooling effect of the impinging oil jet on the second gear is of great importance for its application in a gearbox. This effect is investigated with the C3L and C3R configurations by directing the oil jet onto the non-instrumented gear. With C3L, the instrumented gear completes $\epsilon = 8.6\%$ of the rotation before meshing with the oil jet impinged non-instrumented gear. Similarly, the impingement-meshing distance is $\epsilon = 91.4\%$ for C3R. As mentioned before, the instrumented gear is the driving gear in each case. This means that the impinged flank will be the passive flank of the non-instrumented gear. A conversion of the test rig with drive via the non-instrumented gear could not be realized. However, since the non-impinged flank is also wetted with oil at all operating points with $N = 2000$ RPM, the active flank of the non-instrumented gear will have a considerable oil film present, allowing for the investigation of the heat transfer on the non-impinged instrumented gear. As discussed in Section 3, only the results with $N = 2000$ RPM will be discussed in detail because of the unsuitability of the loss correction approach for the C3 configurations.

Figure 14 shows the $\Delta\bar{h}_{\%}$ values for the C1 and C3 configurations. At $N = 2000$ RPM, it can be seen that for the case closer to a practical application with the lower ϵ, C3L, a lower but still significant secondary heat transfer on the non-impinged gear is present. With the mean value of all measurements at $N = 2000$ RPM considered, the average heat transfer coefficient is 25.86% below the average heat transfer coefficient of the actively impinged gear (configuration C1L). With C3L, a significant amount of the impinged oil volume will be present at the non-instrumented gear during meshing, available to be transferred onto the instrumented gear and participate in the heat transfer with it. Furthermore, some of the oil splashed away or flung off from the non-instrumented gear after the initial impingement, referred to as the secondary oil volume, should also move in the direction of the instrumented gear, increasing the amount of oil available there. With C3R, the secondary oil volume will not be able to reach the instrumented gear, and a limited amount of oil will be available for the heat transfer on the instrumented gear after the rotation, which explains why the average heat transfer coefficient is 62.2% below the average heat transfer coefficient of the actively impinged gear (configuration C1R).

The heat transfer maps of C3R and C3L at OP1 with $\dot{V}_{oil} = 3.2$ L/min and $N = 2000$ RPM are shown in Figs. 10g and h, respectively. The aforementioned effect of the available oil volume is observable in both cases. The s^+ width of the area of increased heat transfer in Fig. 10g corresponds to the area of the active flank that is in contact with the other gear during meshing. The secondary oil volume is also expected to have a relatively low velocity and, therefore, a shallow impingement depth, reaching only the very top of the active flank. The axial uniformity on the active flank of C3L can be attributed to the fact that the opposite side of the contact, the passive flank shown in Fig. 10d, also exhibits good axial uniformity. Additionally, the secondary oil volume will not be as axially concentrated as the cylindrical jet. The low heat transfer with C3R is apparent in Fig. 10g as well. Nevertheless, most

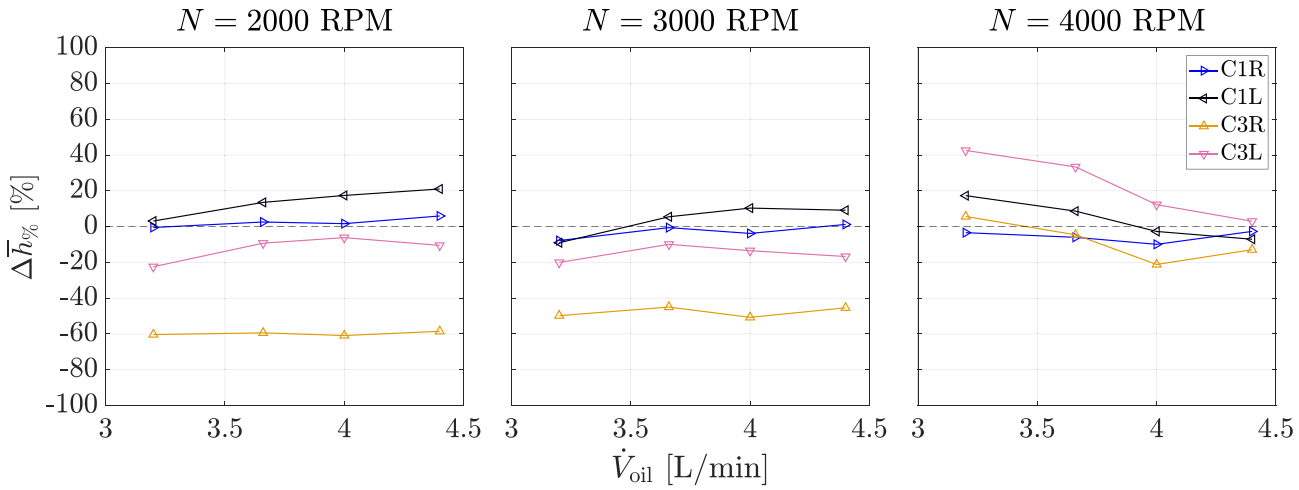

Fig. 14 $\Delta\bar{h}_{\%}$ for configurations C1R, C1L, C3R and C3L

of the heat transfer is still observed on the active flank. The s^+ width of the region with the increased heat transfer coefficient is comparable to C3L and again corresponds to the area which comes in contact with the other gear.

4.3 Comparison of the established impingement methods

In practice, oil jet impingement cooling is realized with an oil jet which is directed:

(I) radially/inclined towards one of the gears (radial/inclined method),
(II) tangentially to the pitch point in the opposite direction of the circumferential velocity (out-of-mesh method),
(III) tangentially to the pitch point in the direction of the circumferential velocity (into-mesh method).

The cooling capacities of these methods can be evaluated with the measurements performed. The relevant values for the cooling performance of Method I depend on the cooling requirements. If the cooling focus lies only on the impinged gear, the measurements with C1L can be utilized (Method IA). However, if both gears are to be cooled by the same oil jet, the total cooling capability can be approximated by averaging the average heat transfer coefficients of configurations C1L and C3L (Method IB). As discussed in Section 3, the comparability of C3 configurations to the others is limited to $N = 2000$ RPM. For Methods II and III, similar cooling capacities can be expected for both gears. Accordingly, the average heat transfer coefficients of C3R and C3L can be used directly for Methods II and III, respectively.

The corresponding $\Delta\bar{h}_{\%}$ values are shown in Fig. 15. All operating points result in decisively higher average heat transfer coefficients with Method I. At two operating points with $N = 4000$ RPM, Methods II and III can barely reach what is achievable with Method IA at $\dot{V}_{\mathrm{oil}} = 4.4$ L/min and $\dot{V}_{\mathrm{oil}} = 3.2$ L/min (OP2), respectively. Method II ensures a higher average heat transfer coefficient than Method III in ten out of twelve operating points with the only exceptions at $\dot{V}_{\mathrm{oil}} = 4.4$ L/min, $N = 3000$ RPM and at $\dot{V}_{\mathrm{oil}} = 4.4$ L/min, $N = 4000$ RPM.

The heat transfer maps with Method II (C4R) at OP1 and OP2 are shown in Figs. 10i and 11i, respectively. At both operating points, the relatively high heat transfer on the active flank is limited only to a small area near the top land. Contrary to that, a comparably high heat transfer is observed on nearly the whole passive flank. This could be attributed to a secondary impact due to splashing, the effect of which should be most significant in Method II since the jet velocity u_{jet} and circumferential velocity of the gear $u_{\mathrm{g,t}}$ are in opposite directions. The relative tangential velocity is thus the maximum achievable at a given operating point. The high amount of splashing would also explain why the wetting on the active flank is extremely limited. In practice, this limited wetting could lead to insufficient cooling of the active flank, where most of the heat is dissipated.

With Method III (C4L) a moderate to high heat transfer is observed on the active flank at both OP1 (Fig. 10j) and OP2 (Fig. 11j). In contrast to the other methods, the gear can be seen as the initiator of the impingement rather than the oil jet. The first tooth tip cuts into the jet and boxes in an oil column between itself and the leading passive flank. The tooth moves into this oil column, which then spreads on the active flank. This results in a relatively homogenous wetting of the active flank in both directions, which is further stimulated by

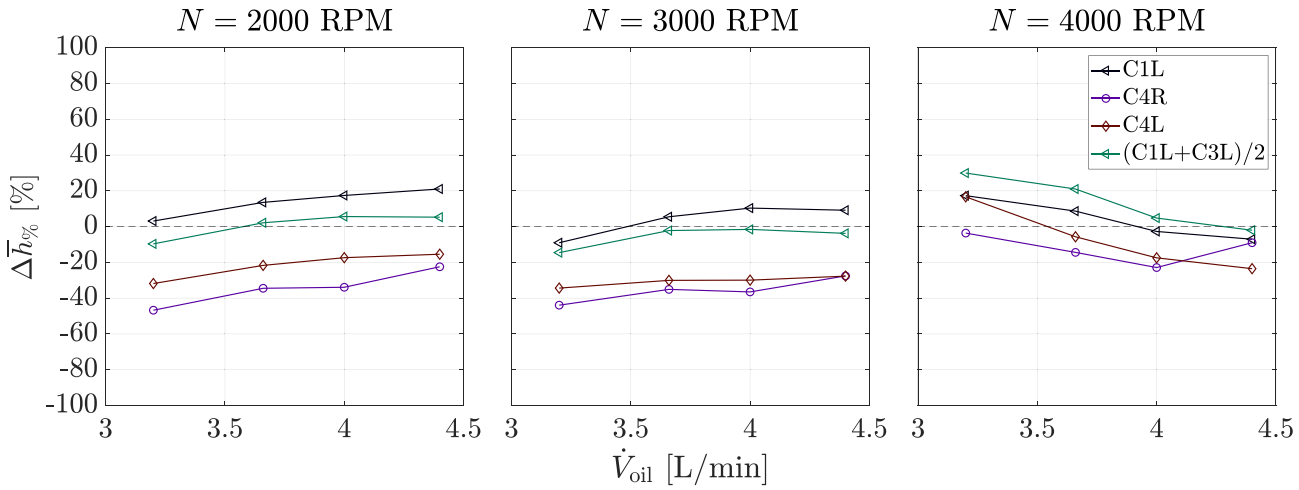

Fig. 15 $\Delta\bar{h}_{\%}$ for configurations Methods IA (C1L), IB ((C1L+C3L)/2), II (C4R) and III (C4L)

meshing, as is the case with C1L. Some parts of the boxed-in oil column can reach the passive flank of the leading tooth if its velocity u_{s} is greater than the circumferential velocity of the tooth $u_{\mathrm{g,t}}$, which is observed at OP1. A region of increased heat transfer is axially centred on the passive flank showing the direct impingement. This also explains the relatively low heat transfer on the active flank compared to OP2, where the whole oil column impinges on the active flank.

5 Conclusion and outlook

A total of ten different configurations with and without meshing are investigated in order to draw conclusions about the influence of meshing on the heat transfer with inclined oil jet impingement, the cooling effect on the non-impinged gear with inclined oil jet impingement and most importantly, the comparison of established cooling methods.

No significant effect of meshing on the average heat transfer coefficient with the inclined impingement is found. However, as the distance between impingement and meshing decreases, the heat transfer coefficient distribution becomes more uniform in the axial direction. An increase in the rotational speed further enhances this effect.

When the impingement and meshing locations are close together, high heat transfer coefficients are observed on the non-impinged gear. The area of the tooth surface with increased heat transfer is the area coming in contact with the impinged tooth. At the maximum distance between impingement and meshing locations, the heat transfer on the non-impinged gear is very low. These conclusions are only limited to the lowest rotational speed of 2000 RPM investigated since the implemented loss correction is not suited for higher rotational speeds.

The inclined impingement method is superior to the other established alternatives regarding the average heat transfer coefficient as well as its spatial distribution. The out-of-mesh method performs the worst in nearly all of the operating points. The average heat transfer coefficient is lower than its alternatives, and the heat transfer is almost exclusively concentrated on the passive flank, away from where the heat dissipation is expected to occur. With into-mesh impingement, the wetting of the active flank is comparable to what is achievable with the inclined impingement method. The oil jet velocity should be adjusted to the rotational speed of the gear if the impingement on the passive flank is to be limited for a more concentrated cooling of the active flank. In addition to these findings, the heat transfer with the inclined impingement method could be further optimized depending on the rotational speed and the oil volume flow rate by changing the jet inclination. This is only possible to a limited extent with the out-of-mesh and into-mesh methods.

The implemented loss correction approach is based on multiple assumptions, which are challenging to validate. The accuracy of the results could be improved by investigating and understanding the occurring losses and heat dissipation in more detail. However, a meticulous investigation of these phenomena and their influence on heat transfer is experimentally and numerically extremely challenging.

The investigation in this study was aimed to deliver a novel insight into the cooling aspect of oil jet impingement in meshing gears isolated from other heat sources found in the real world application. It would be a great addition to the state of research if experiments with realistic loads were conducted to test whether the measured temperatures align with the expectations regarding cooling potentials of the investigated configurations.

Acknowledgements Bundesministerium für Wirtschaft und Klimaschutz (BMWK) and Rolls-Royce Deutschland Ltd. and Co. KG have funded the research activities leading to this study within the framework of research program Luftfahrtforschungsprogramm 5 (Project No. 20T1729). The financial support is gratefully acknowledged by the authors.

Author contributions E.A. wrote the manuscript and all authors commented and revised it. All authors read and approved the final manuscript to be published. Experimental design, software development, model development, data analysis and interpretation were carried out by E.A.. C.K. contributed to the design and instrumentation of the experimental setup and conduction of experiments. C.S. and H.J.B. were responsible for the funding acquisition. All authors contributed to the conception and design of the work.

Funding Open Access funding enabled and organized by Projekt DEAL.

Data availability The data supporting this study cannot be made publicly available due to a confidentiality agreement with one of the funding bodies. However, anonymized data may be available upon request and with permission from the relevant funding body.

Declarations

Competing interests The authors declare no competing interests.

References

1. Townsend DP, Akin LS (1981) Gear lubrication and cooling experiment and analysis. J Mech Design 103(4):219–226
2. Schober H (1983) Einspritzschmierung bei Zahnradgetrieben. Dissertation, Universität Stuttgart, Stuttgart
3. Leoni P (1991) Hochleistungsgetriebe mit getrennter Schmierung und Kühlung. Dissertation, Universität Stuttgart, Stuttgart
4. Handschuh R (1992) Effect of lubricant jet location on spiral bevel gear operating temperatures. NASA Technical Memorandum 105656, Lewis Research Center, Cleveland, Ohio
5. Handschuh R (1995) Thermal behavior of spiral bevel gears. NASA Technical Memorandum 106518, Lewis Research Center, Cleveland, Ohio
6. Wang Y, Tang W, Chen Y, Wang T, Li G, Ball AD (2017) Investigation into the meshing friction heat generation and transient thermal characteristics of spiral bevel gears. Appl Therm Eng 119(11):245–253. https://doi.org/10.1016/j.applthermaleng.2017.03.071
7. Zhang J-G, Liu S-J, Fang T (2017) Determination of surface temperature rise with the coupled thermo-elasto-hydrodynamic analysis of spiral bevel gears. Appl Therm Eng 124(5):494–503. https://doi.org/10.1016/j.applthermaleng.2017.06.015
8. Gan L, Xiao K, Wang J, Pu W, Cao W (2019) A numerical method to investigate the temperature behavior of spiral bevel gears under mixed lubrication condition. Appl Therm Eng 147:866–875. https://doi.org/10.1016/j.applthermaleng.2018.10.125
9. Wang Y, Niu W, Chen Y, Song G, Tang W (2016) Convection heat transfer and temperature analysis of oil jet lubricated spur gears. Ind Lubr Tribol 68(6):624–631. https://doi.org/10.1108/ILT-10-2015-0145
10. Li W, Tian J (2017) Unsteady-state temperature field and sensitivity analysis of gear transmission. Tribol Int 116:229–243. https://doi.org/10.1016/j.triboint.2017.07.019
11. Fernandes CM, Rocha DM, Martins RC, Magalhães L, Seabra JH (2018) Finite element method model to predict bulk and flash temperatures on polymer gears. Tribol Int 120:255–268. https://doi.org/10.1016/j.triboint.2017.12.027
12. Hu X, Chen J, Wu M, Wang J (2021) Thermal analysis of herringbone gears based on thermal elastohydrodynamic lubrication considering surface roughness. Energies 14(24):8564. https://doi.org/10.3390/en14248564
13. von Plehwe FC, Schwitzke C, Bauer HJ (2021) Heat transfer coefficient distribution on oil injection cooled gears: experimental method, uncertainty and results. J Tribol 143(9):091201. Published Online: January 8, 2021
14. Ayan E, von Plehwe FC, Keller MC, Kromer C, Schwitzke C, Bauer H-J (2022) Experimental determination of heat transfer coefficient on impingement cooled gear flanks: validation of the evaluation method. J Turbomach 144(8):229. https://doi.org/10.1115/1.4053694
15. Ayan E, Kromer C, Schwitzke C, Bauer HJ (2022) Experimental investigation of the oil jet heat transfer on meshing spur gears. 25th Conference of International Society on Air Breathing Engines, Ottawa, Canada, September 25–30, 2022. ISABE
16. Glahn A (1995) Zweiphasenströmung in Triebwerkslagerkammern - Charakterisierung der Ölfilmströmung und des Wärmeübergangs. Dissertation, Universität Karlsruhe
17. von Plehwe FC (2021) Untersuchung des Wärmeübergangs durch Einspritzkühlung für ein Höchstleistungsgetriebe. Dissertation, Karlsruher Institut für Technologie (KIT), Logos Verlag Berlin
18. Keller MC, Kromer C, Cordes L, Schwitzke C, Bauer H-J (2020) CFD study of oil-jet gear interaction flow phenomena in spur gears. Aeronaut J 124(1279):1301–1317. https://doi.org/10.1017/aer.2020.44
19. Akin LS, Townsend DP, Mross JJ (1975) Study of lubricant jet flow phenomena in spur gears. NASA Technical Memorandum 71572, Lewis Research Center, Cleveland, Ohio